Title

Combining hyperpolarized 13C MRI with a liver-specific gadolinium contrast agent for selective assessment of hepatocyte metabolism

Journal

Magnetic Resonance in Medicine, 77(6)

ISSN

0740-3194

Authors

Ohliger, Michael A
von Morze, Cornelius
Marco-Rius, Irene
et al.

Publication Date

2017-06-01

DOI

10.1002/mrm.26296

Peer reviewed

HHS Public Access

Author manuscript

Magn Reson Med. Author manuscript; available in PMC 2017 June 01.

Published in final edited form as:

Magn Reson Med. 2017 June ; 77(6): 2356–2363. doi:10.1002/mrm.26296.

Combining Hyperpolarized ^{13}C MRI With a Liver-Specific Gadolinium Contrast Agent for Selective Assessment of Hepatocyte Metabolism

Michael A. Ohliger*, **Cornelius von Morze**, **Irene Marco-Rius**, **Jeremy Gordon**, **Peder E. Z. Larson**, **Robert Bok**, **Hsin-yu Chen**, **John Kurhanewicz**, and **Daniel Vigneron**

Department of Radiology and Biomedical Imaging, University of California, San Francisco, San Francisco, CA

Abstract

Purpose—Hyperpolarized ^{13}C MRI is a powerful tool for studying metabolism, but can lack tissue specificity. Gadoxetate is a gadolinium-based MRI contrast agent that is selectively taken into hepatocytes. The goal of this project was to investigate whether gadoxetate can be used to selectively suppress the hyperpolarized signal arising from hepatocytes, which could in future studies be applied to generate specificity for signal from abnormal cell types.

Methods—Baseline gadoxetate uptake kinetics were measured using T_1-weighted contrast enhanced imaging. Relaxivity of gadoxetate was measured for [1-^{13}C]pyruvate, [1-^{13}C]lactate, and [1-^{13}C]alanine. Four healthy rats were imaged with hyperpolarized [1-^{13}C]pyruvate using a three-dimensional (3D) MRSI sequence prior to and 15 min following administration of gadoxetate. The lactate:pyruvate ratio and alanine:pyruvate ratios were measured in liver and kidney.

Results—Overall, the hyperpolarized signal decreased approximately 60% as a result of pre-injection of gadoxetate. In liver, the lactate:pyruvate and alanine:pyruvate ratios decreased 42% and 78%, respectively (P <0.05) following gadoxetate administration. In kidneys, these ratios did not change significantly. Relaxivity of gadoxetate for [1-^{13}C]alanine was 12.6 times higher than relaxivity of gadoxetate for [1-^{13}C]pyruvate, explaining the greater selective relaxation effect on alanine.

Conclusions—The liver-specific gadolinium contrast-agent gadoxetate can selectively suppress normal hepatocyte contributions to hyperpolarized ^{13}C MRI signals.

Keywords

hyperpolarized carbon; liver; gadoxetate; pyruvate; metabolism

INTRODUCTION

Hyperpolarized ^{13}C MRI is a promising tool for investigating metabolic pathways in vivo with successful initial applications in a variety of diseases, including cancer (1),

*Correspondence to: Michael A. Ohliger, M.D., Ph.D., Box 0628, 1001 Potrero Ave. SFGH 1x60, San Francisco, CA 94110. michael.ohliger@ucsf.edu.

cardiovascular diseases (2,3), inflammation (4), and diabetes (5). However, the hyperpolarized signal can lack cellular specificity. In the injured liver (6), for example, it is currently not possible to determine whether the observed hyperpolarized signal comes from hepatocytes or from inflammatory cells. Similarly, because of the limited spatial resolution of most hyperpolarized ^{13}C MRI studies, it is likewise problematic to separate the signal arising from small tumors from surrounding nontumorous hepatocytes, which often have high metabolic activity. Therefore, this project was designed to investigate the possibility of using a liver-specific contrast agent to selectively suppress hyperpolarized signals arising from normal hepatocytes. This approach could in future studies be applied to distinguish hyperpolarized signals arising from normal hepatocytes from other abnormal cell types associated with liver disease.

Gadoxetic acid is an FDA-approved gadolinium-based contrast agent (GBCA) that is taken into hepatocytes through facilitated transport by the organic anion-transporting polypeptide 1 (OATP1) and actively excreted into the biliary system by the multidrug resistant protein 2 (MRP2) (7–9). Approximately 50% of the agent is cleared through the biliary system and 50% is cleared through the kidneys. This agent is used clinically to detect liver metastases as well as hepatocellular carcinoma (90% of which lack the required transporter for gadoxetate) (10). Gadoxetate has been administered to more than 2.2 million patients (11). When gadoxetate is used clinically, T_1-weighted images are usually acquired during the “hepatobiliary phase” of enhancement, which occurs 10–15 min after injection of contrast. In the hepatobiliary phase, there is maximal contrast between the hyperintense liver and hypointense blood vessels. Because contrast is only taken up by hepatocytes, tumors appear as hypointense foci within an otherwise bright liver (12).

In this study we proposed to exploit the cellular specificity of gadoxetate in order to achieve targeted hyperpolarized ^{13}C MR imaging and spectroscopy. Because most gadoxetate resides within hepatocytes, intracellular hyperpolarized ^{13}C metabolites should have much shorter T_1 relaxation times than hyperpolarized ^{13}C metabolites located within other cell types or within the vasculature. Therefore, gadoxetate should provide suppression of hyperpolarized signals that are hepatocyte specific.

This study was designed to investigate the feasibility of this approach by performing hyperpolarized ^{13}C MR spectroscopic imaging (MRSI) in healthy normal rats with three goals: First, we sought to measure the relaxivities of gadoxetate for [1-^{13}C]pyruvate and its metabolites, [1-^{13}C]alanine, and [1-^{13}C]lactate. Second, we aimed to determine whether high-quality hyperpolarized ^{13}C spectra could be obtained following gadoxetate injection despite the presence of residual circulating gadolinium. Third, we attempted to measure the selective suppression of hyperpolarized ^{13}C metabolite signal arising from the liver in comparison to the kidney, where gadoxetate was expected to be purely extracellular.

METHODS

MR Imaging Protocol

All MR experiments were performed using a 3 Tesla (T) clinical MRI scanner (MR Discovery 750, GE Healthcare, Waukesha, Wisconsin) equipped with broadband amplifiers

and a custom-built dual tuned $^{1}H/^{13}C$ transmit/ receive radiofrequency (RF) volume coil. Animal experiments were performed using a volume insert coil designed to image rats.

Relaxivity Measurements

The relaxivities of gadoxetate for [1-^{13}C]pyruvate, [1-^{13}C]alanine, and [1-^{13}C]lactate were determined by measuring the spin lattice relaxation rate, R_1, for each compound in the presence of varying concentrations of gadoxetate.

Pure [1-^{13}C]pyruvic acid or [1-^{13}C]lactic acid samples were mixed with 15 mM OX63 trityl radical and 1.5 mM Dotarem (Guerbet, Roissy, France), and then polarized for 1–2 h in a 3.35T Hypersense dynamic nuclear polarization (DNP) polarizer (Oxford Instruments, Tubney Woods, UK). The hyperpolarized samples were then warmed and dissolved to a concentration of 24 mM as a neutral solution in a NaOH/Tris buffer.

Relaxivities of gadoxetate with respect to [1-^{13}C]pyruvate and [1-^{13}C]lactate were measured by mixing hyperpolarized material with different aqueous dilutions of gadoxetate (Bayer Pharmaceuticals, gadoxetate concentration range 0–0.25 mM). These tubes were placed within the RF coil and arranged in a linear fashion in the superior-inferior (z) direction. A spatial gradient was applied along the z-direction to localize the signal from each tube. Spectra were then acquired every 3 s using nonselective RF pulses and a flip angles of 5°. The total signal from each tube was integrated at each time point, corrected for the 5° flip angle, and fit to the exponential function $\exp(-R_1 t)$, in which R_1 is the spin-lattice relaxation rate in units 1/s.

Hyperpolarized [1-^{13}C]alanine was prepared as previously described (13) using a mixture of 350 mg [1-^{13}C] L-alanine (Cambridge Isotope Laboratories, Andover, Massachusetts), 250 μl 18.94 M NaOH, 100 μl DMSO, and 15 mM OX63 trityl radical. The preparation was polarized for 2 h and then dissolved in a phosphate buffer containing 0.3 mM Na_2EDTA (ethylenediaminetetraacetic acid disodium salt) with HCl added to neutralize the NaOH for a final concentration of 75 mM. Aqueous T_1 of [1-^{13}C]alanine at 3 T was measured by performing a pulse-and-acquire pulse sequence using a nonselective 5° pulse every 3 s. The signal integral at each time point was fit to an exponential decay as described previously.

Although we were successful in measuring the T_1 of [1-^{13}C]alanine without added gadoxetate using a hyperpolarized sample, mixtures of hyperpolarized [1-^{13}C]alanine and gadoxetate did not yield sufficient signal-to-noise ratio (SNR) for reliable measurement. Therefore, we were not able to use the hyperpolarized sample to measure directly the relaxivity of gadoxetate with respect to alanine. Instead, a non-hyperpolarized saturation-recovery measurement was performed using a sample containing 4 mL of enriched [1-^{13}C]alanine (Isotec, Sigma-Aldrich, St. Louis, Missouri) dissolved in phosphate-buffered saline (total alanine concentration 1.2 M, pH 6.5). To increase sensitivity, a smaller (~5 cm) transmit-receive dual-tuned RF coil was used. A saturation-recovery experiment was performed using three successive 90° saturation pulses, followed by a delay of 0.1–240 s, followed by a 90° nonselective excitation pulse. The signal for each delay was integrated and fit to the equation $a*(1-\exp(-R_1*t_{del}))$, where t_{del} is the saturation-recovery delay time. Fitting was performed using a nonlinear fit and Levenberg-Marquart algorithm. This

experiment was performed and R_1 was measured using four different concentrations of gadoxetate: 0, 0.025, 0.05, and 0.075 mM.

For each compound, the relaxivity was computed as the slope of the spin-lattice relaxation rate, R_1, versus gadoxetate concentration.

Animal Handling

Healthy Sprague-Dawley rats (Indianapolis, Indiana) were imaged under a protocol approved by our local institutional animal care and use committee. Continuous isoflurane gas was administered (1.5%, flow rate 1 L/ min) for anesthesia during the experiments. Animals were kept warm using a heated water pad and were monitored continuously.

Hyperpolarization for In Vivo Studies

For each hyperpolarized ^{13}C injection, approximately 32 mg of a mixture of [1-^{13}C]pyruvic acid with 15 mM OX63 trityl radical and 1.5 mM Dotarem (Guerbet, Roissy, France) was polarized through DNP using either a 3.35 T Hypersense polarizer or a 5T SpinLab polarizer (Research Circle Technology, Albany NY). Polarization times were at least 1 h at 3.35 T and at least 2 h at 5 T. After polarization, pyruvic acid was rapidly warmed, neutralized, and dissolved to a final concentration of approximately 80 mM. For each hyperpolarized experiment, approximately 2.5 mL of 80 mM hyperpolarized pyruvate solution was injected over 12 s through the rat's tail vein.

Timing of Gadoxetate Administration for Hyperpolarized ^{13}C Experiment

The time between the injection of gadoxetate and the hyperpolarized ^{13}C experiment was an important consideration. Ideally, we aimed to achieve maximum suppression of signal from liver parenchyma (maximal intracellular gadoxetate), while minimizing the suppression of circulating ^{13}C pyruvate within the bloodstream (minimal intravascular gadoxetate). This is a similar consideration to the one that is made when choosing the imaging time for clinical applications of gadoxetate. The hepatobiliary phase of contrast administration occurs when there is maximal T_1-weighted contrast among the liver, vasculature, and tumors. Clinically, the hepatobiliary phase is usually obtained 15–20 min after gadoxetate injection (10). A large retrospective imaging review has shown that 80% of patients achieve optimal hepatobiliary phase timing within 15 min (14). Previously published studies in mice (15) similarly showed peak liver enhancement on T_1-weighted images enhanced with gadoxetate occurring at 15–20 min.

Dynamic Contrast Enhancement Measurements

To determine the optimal time after gadoxetate administration to perform hyperpolarized ^{13}C acquisition, we measured the dynamics of liver enhancement with gadoxetate within the rat liver. First, T_1 was measured by obtaining three-dimensional (3D) T1-weighted spoiled gradient echo (SPGR) images using multiple flip angles (spectral fat saturation; echo time (TE) 1.5 ms; repetition time (TR) 4.9 ms; matrix 160 × 160 × 20; field of view (FOV) 10 × 10 cm; slice thickness 2.5 mm; flip angles 3, 6, 12, and 15°). Next, 0.1 mmol/kg gadoxetate was injected into the rat's tail vein and 3D T_1-weighted volumes were acquired every minute with the same parameters as previously and a flip angle of 12°.

Images were imported into OsiriX (16) and processed using the DCE Tool plugin (kyungs.bol.ucla.edu/software/DCE_tool/DCE_tool.html). T_1 maps were generated from the multiple flip angle data and then used to calculate T_1 at each time point, which was then used to estimate contrast agent concentration at each time point. T_1 values were converted to concentrations using the known plasma relaxivity of gadoxetate at 3 T of 6.0 mM^{-1} s^{-1} (17). Regions of interest were drawn over the liver parenchyma and inferior vena cava (IVC). These data (see "Results" section), together with experience in clinical imaging with gadoxetate, led us to choose an optimal hyperpolarized ^{13}C imaging time of 15 min following gadoxetate administration.

Multislab Dynamic ^{13}C Experiments

The dynamic time course of metabolite production under the influence of gadoxetate was measured in three rats. Beginning approximately 20 s after the start of pyruvate injection, localized spectra were acquired from two 2.0-cm axial slabs, one placed over the liver and one placed over the kidneys. Ten spectra were acquired from each slab with a flip angle of 20° and temporal resolution of 3 s, for a total acquisition time of 30 s. Identical dynamic experiments were performed before and 15 min following the injection of gadoxetate at a concentration of 0.1 mmol/kg. The timing of imaging was chosen to match the human hepatobiliary phase of contrast enhancement using gadoxetate (15–20 min) as well as dynamic contrast enhancement images performed in normal rats (see previously). The timing of the multislab dynamic experiments is shown graphically in Figure 1a.

3D Localized ^{13}C Experiments

To minimize partial volume effects, spatially localized spectroscopic images were obtained using a 3D echo planar spectroscopic imaging (EPSI) sequence with double spin echo refocusing (5,18). Images were acquired with 8 × 8 × 8mm voxels and a matrix size of 18 × 10 × 8, with TR = 215 ms, TE = 140 ms, progressive flip angle (19), and spectral width 543 Hz. Data were acquired beginning 22 s after pyruvate injection with a total imaging time of 17 s.

Four rats were imaged. For each rat, four serial hyperpolarized injections were performed in a single imaging session (Fig. 1b). The first data set was collected before injection of gadoxetate. The next three data sets were acquired after injection of gadoxetate in the early phase (1–3 min), hepatobiliary phase (15 min), and delayed phase (25 min). To perform rapid serial injections in an efficient manner, samples were polarized simultaneously using two different polarizers. A 3.35T Hypersense polarizer was used for injections 1 and 4. A 5T SpinLab polarizer was used for injections 2 and 3. Because of technical issues, acquisition of time points 2 (early) and 4 (late delayed) failed in 2/4 animals. All four animals had a successful acquisition of time point 1 (pre-gadolinium) and time point 3 (15 minute hepatobiliary phase). Because the 15-min time point most closely matched the hepatobiliary phase in normal human liver, and because all four experiments succeeded at this time point, these data were used for quantitative analysis. The spectra from the other two time points, which were not obtained in high enough numbers to be statistically reliable, were used qualitatively below.

^{1}H MRI Reference Images

Anatomic reference images were acquired using a 3D steady-state free precession (SSFP) sequence with the following parameters: TE = 2.2 ms, TR = 5.5 ms, flip angle = 50°, FOV = 16 × 8 × 4.5 cm, matrix = 256 × 128 × 76, NEX = 3. To confirm the arrival of contrast, T_1-weighted 3D spoiled GRE images were obtained before gadoxetate administration and following the last pyruvate injection with the following parameters: TE = 2.8 ms TR = 6.8 ms, flip angle = 10°, FOV = 10 cm, matrix = 256 × 224, 120 slices, slice thickness = 2 mm.

Data Analysis

Data were reconstructed and analyzed offline using MATLAB (MathWorks, Natick, Massachusetts). In all cases, absolute magnitude spectra were analyzed. 3D spectra were corrected for B_0 inhomogeneity by shifting the spectra in the frequency dimension so that the pyruvate peaks were at the same spectral positions in all voxels. The areas under the pyruvate, alanine, and lactate peaks were computed. For 3D data sets, the metabolite signals were interpolated in the spatial dimension using MATLAB to match the resolution of the anatomic images and then fused onto the T_2-weighted SSFP anatomic images using Osirix 5.0 (16) and SIVIC (10,20). Using the proton images, regions of interest (ROIs) were drawn over either the center liver slices and center kidney slices (separate ROIs were placed on each kidney). The average signal from each ROI was recorded. To account for possible shot-to-shot differences in polarization, metabolite signals were quantified using the lactate-to-pyruvate and alanine-to-pyruvate ratios.

Statistical Analysis

Statistics were computed using Prism 6 software (Graph-pad, San Diego, California). Mean metabolite-to-pyruvate ratios before and after gadolinium administration were compared using unpaired t-tests. A *P*-value of less than 0.05 was taken to confer statistical significance.

RESULTS

^{13}C relaxivity of Gadoxetate

Relaxation rates of pyruvate, alanine, and lactate as a function of gadoxeate concentration were plotted as a function of gadolinium concentration (Fig. 2). Relaxivity was estimated by determining the slope of the relaxation rate, R_1, versus gadoxetate concentration for each compound (Table 1). In solution at 3 T, the relaxivity of gadoxetate for [1-^{13}C]lactate was approximately 1.4 times higher than the relaxivity for [1-^{13}C]pyruvate, although this change was not statistically significant. In contrast, the relaxivity of gadoxetate for [1-^{13}C]alanine was 12.6 times higher than the relaxivity for pyruvate, and the relaxivity was 9 times higher for [1-^{13}C]alanine than it was for [1-^{13}C]lactate (both changes were statistically significant with $P<0.05$).

To account for potential effects of high alanine concentration on our relaxivity measurements, we measured the R_1 of [1-^{13}C]alanine without gadolinium using a hyperpolarized sample at 75 mM. R_1 of [1-^{13}C]alanine was 0.035 s^{-1} (95% confidence interval 0.032–0.038 s^{-1}), which was not significantly different from the high-concentration

thermal measurement made using a thermally polarized sample containing 1.2 M [1-^{13}C]alanine, which was 0.033 s^{-1} (95% confidence interval 0.030–0.036 s^{-1}).

Anatomic Imaging

T_1-weighted images that were acquired before and following gadoxetate administration (Fig. 3) showed the expected liver enhancement pattern. The liver parenchyma was uniformly hyperintense (caused by accumulated gadoxetate) with hypointense vasculature (Fig. 3c). Contrast was observed within the common bile duct (Figs. 3d and 3e), in keeping with the expected biliary excretion of gadoxetate. The imaging pattern was identical to the hepatobiliary phase of gadoxetate contrast observed when imaging humans (12).

Contrast Kinetics

Estimated concentration of gadoxetate was measured in an ROI placed over the central liver and compared with the concentration within an ROI placed over the inferior vena cava (IVC). Within the IVC (Fig. 4), the gadoxetate rose sharply and then fell as it was cleared from the bloodstream, with much of the bloodstream gadoxetate eliminated within 5–10 min. By contrast, gadoxetate concentration within the liver fell slowly, reflecting accumulation within hepatocytes and slow biliary excretion. Although gadoxetate within the IVC was already close to baseline by 5–10 min, we chose an imaging time of 15 min to allow a further margin of safety, further minimizing blood pool gadoxetate that may cause relaxation of our injected ^{13}C pyruvate.

Multslab Dynamic ^{13}C Spectra

Dynamic spectra were acquired every 3 s from slabs placed over the kidney and liver (Fig. 5a). Slab spectra were acquired before and 15 min following gadoxetate administration (Fig. 1a). The summed spectra taken over all time points (Fig. 5b) showed the expected global decrease in hyperpolarized signal caused by the presence of blood pool gadolinium contrast in both the kidney and the liver. Average total pyruvate signal after gadolinium administration compared with before gadolinium administration was 39.2% in the kidney (standard error 8%) and 42% in the liver (standard error 11%, not statistically different from kidney). Dynamic time curves observed for a single animal are shown in Fig. 5c. After contrast administration, there was expected faster decay at late time points, consistent with overall shorter T_1 relaxation times. The early points of the decay curve in the liver were qualitatively different before and after contrast administration, particularly for alanine. These effects are shown quantitatively in Fig. 5d, by comparing the relative area under the time curve for each metabolite. The average change in alanine:pyruvate ratio within the liver following gadolinium administration was significantly lower than the change in alanine:pyruvate ratio within the kidney. The change in lactate:pyruvate ratio following gadolinium was not significantly different in the liver or kidney.

Spatially Resolved Measurement

To achieve better spatial localization, 3D EPSI acquisitions were obtained before and after gadoxetate administration, with timing shown in Figure 1b. Because the samples used in acquisitions 1 and 4 (pre-gadolinium and 25-min time points) were polarized at 3.35 T, and

the samples used for acquisitions 2 and 3 (1 min and 15 min) were polarized at 5 T, they had different overall polarization levels. Therefore, at every point, spectra were normalized so that the pyruvate peaks had the same amplitudes. Individual spectra obtained from single voxels placed over the liver and kidney (Fig. 6) demonstrated a pattern in which initially (1 min) all metabolite signals were reduced in both the kidney and the liver. At 15 min (hepatobiliary phase), the lactate signal partially recovered in the liver but the alanine signal remained suppressed. In the kidney, the metabolite ratios recovered to a level similar to that seen before gadoxetate administration.

Metabolite changes were quantified by drawing ROIs over the midslice of the liver, right kidney, and the left kidney. Metabolite ratios were measured as ratios of lactate and alanine to pyruvate. In the liver, the lactate:-pyruvate ratio (Fig. 7a) decreased by 42% and the alanine:pyruvate ratio (Fig. 7b) decreased by 78% (both $P<0.05$). In contrast, neither the lactate:pyruvate ratio nor the alanine:pyruvate ratio changed significantly in either kidney.

DISCUSSION

The results of this study demonstrate that the liver-specific gadolinium contrast agent, gadoxetate, can be used to selectively suppress hyperpolarized ^{13}C signal arising from liver when compared with the kidneys. At 15 min after gadoxetate administration, alanine was suppressed on average 78%, and lactate was suppressed on average 42% in the liver, whereas changes in the kidney were not statistically significant. This observation was consistent with our expectations that gadolinium within hepatocytes should have a preferential relaxation effect on alanine produced within those hepatocytes.

The results derived from slab dynamic experiments (Fig. 5d) were slightly different than those derived from the 3D EPSI experiments (Fig. 7). For example, in the 3D EPSI experiments, we found a significant decrease in liver lactate after gadoxetate was administered, and no significant change in lactate arising from the kidneys. However, in the slab experiments, the changes were insignificant in both liver and kidneys. These differences can likely be attributed to two causes. First, in the slab dynamic experiments, we measured the total area under the time course curve for each metabolite, whereas for the 3D EPSI experiments, measurements were made at a specific time. Second, the slab experiments were subject to significant partial volume effects. Both the liver and kidney slabs contained a large amount of vasculature. In addition, the kidney slabs contained significant amounts of bowel.

The measured solution-state relaxivity of gadoxetate for [1-^{13}C]pyruvate (0.087 +/−0.023 $mM^{-1}\ s^{-1}$) was lower than the relaxivity that has been observed for water imaging with gadoxetate (5.9–6.1 $mM^{-1}\ s^{-1}$ in plasma at 3 T) (17). This difference in relaxivity between [1-^{13}C]pyruvate and water is likely the result of two effects: First, the gyromagnetic ratio of ^{13}C is approximately 1/4th that of ^{1}H; and second, inner sphere relaxation is hindered because of the increased size of pyruvate (compared with water), and outer sphere relaxation is reduced because of the negative charge of pyruvate. Similarly reduced relaxivities compared with water have been observed using gadodiamide for the C_1 and C_5 carbons of glutamate (0.42 and 0.55 $mM^{-1}\ s^{-1}$ at 9.4 T, respectively) (21).

Interestingly, the solution-state relaxivities of gadoxetate for [1-^{13}C]lactate and for [1-^{13}C]alanine were greater than they were for [1-^{13}C]pyruvate. Alanine in particular had nearly 12 times faster spin lattice relaxation per mole gadoxetate than [1-^{13}C]pyruvate. It is uncertain why alanine relaxation occurred much more efficiently in the presence of gadoxetate than either lactate or pyruvate. Presumably, the zwitterionic form of alanine permitted it to interact much more closely with gadoxetate than the other compounds. Regardless, the fact that the metabolites of [1-^{13}C]pyruvate relaxed faster than [1-^{13}C]pyruvate itself in the presence of gadoxetate potentially benefits this approach. Less of the circulating blood pool [1-^{13}C]pyruvate is relaxed, but once the [1-^{13}C]pyruvate is metabolized by the tissues, gadoxetate could potentially produce larger contrast in the metabolite signal between liver and nonliver tissues.

One potential confounding factor in the relaxivity measurements is that the relaxivity of [1-^{13}C]alanine was measured using a higher concentration than the relaxivity of [1-^{13}C]lactate and [1-^{13}C]pyruvate. This high concentration was necessary to provide sufficient signal for relaxivity measurements of thermally polarized samples. We were not able to measure relaxivity of [1-^{13}C]alanine directly using a low-concentration hyperpolarized sample (as we had done for pyruvate and lactate), because mixtures of hyperpolarized [1-^{13}C]alanine and gadoxetate did not yield sufficient signal to noise for reliable measurements. Higher concentrations of alanine are known to have increased viscosity (22), which could potentially cause a decrease in R_1. However, we were able to measure R_1 of hyperpolarized [1-^{13}C]alanine at 75 mM, which was nearly identical to the R_1 measured at 1.2 M. Although we cannot rule out the possibility that viscosity could have a larger effect at higher gadoxetate concentrations, the similar R_1 in samples with zero gadolinium is reassuring.

The selective suppression of ^{13}C signal arising from normal hepatocytes that was demonstrated in this study has several potential applications to be further explored in future studies. As a basic science tool, this method may help to determine whether ^{13}C metabolites observed in hyperpolarized experiments are produced by hepatocytes or other cells. More significantly, gadoxetate is not taken up by liver metastases or most hepatocellular carcinomas (10,14). By selectively suppressing the ^{13}C signal from normal liver, this method may eventually improve the assessment of tumor metabolism. Indeed, background liver signal suppression is not possible using competing molecular imaging modalities such as FDG-PET, in which high background metabolic activity can obscure small tumors (23). If successful, this would suggest a unique advantage for hyperpolarized ^{13}C compared with FDG-PET.

In assessing the gadolinium-related changes in ^{13}C signal, we used the kidneys as reference standards for organs where gadoxetate was extracellular. The kidneys were chosen because they have high metabolic signals and they do not incorporate gadoxetate intracellularly. However, the kidneys are an imperfect reference because gadoxetate is 50% excreted through the kidneys, causing gadoxetate to be more highly concentrated in the kidneys than it is in other organs 15 min after injection. Therefore, the relative effects on metabolites may be overestimated. However, in this study using normal rats, we were limited because the kidneys were one of the few organs other than liver that showed high enough levels of

metabolites to measure changes reliably. Future experiments in tumor models and ultimately patients are required to investigate the value of this approach for suppressing hepatocyte signals to benefit studies of liver disease.

One limitation of using gadolinium agents to increase selectivity in hyperpolarized ^{13}C imaging is that a portion of ^{13}C signal is lost as a result of interactions with gadolinium, which is still circulating within the blood. In this study, approximately 60% of the overall pyruvate signal was lost. However, there was sufficient signal remaining to detect metabolites and obtain high-quality spectra. Gadoxetate is particularly well suited to this type of experiment because its plasma half-life is relatively short compared with other gadolinium agents that do not have biliary excretion. The low gadoxetate relaxivity for [^{13}C]pyruvate (discussed previously) also likely contributes to our ability to observe significant hyperpolarized ^{13}C signal despite blood pool relaxation.

The dose of gadoxetate used in this study (0.1 mmol/ kg) was greater than the FDA-approved clinical dose of gadoxetate (0.025 mmol/kg). We chose this higher dose to have a positive control, so we could be confident in seeing an effect. In future studies, we intend to test whether smaller doses can still provide suppression of liver metabolite signals. A decreased dose of gadoxetate may also potentially decrease the blood pool effects on the hyperpolarized signal. Although the dose used was higher than the standard clinical dose of gadoxetate, it is equivalent to the gadolinium concentration given clinically with other gadolinium-based contrast agents such as gadopentetate, which are often given at doses as high as 0.1 mmol/kg (24). Therefore, this dose would be reasonable for future human applications.

Previous studies have explored the use of gadolinium contrast agents to distinguish the intravascular and extravascular hyperpolarized ^{13}C signal (25,26). To our knowledge, our study is the first example of selective gadolinium agents being used to selectively suppress hyperpolarized signals from a certain cell type.

CONCLUSIONS

A liver-specific gadolinium-based contrast agent can be used to increase the organ selectivity of hyperpolarized ^{13}C MRI experiments by selectively suppressing the signal arising from hepatocytes.

Acknowledgments

This study was funded by grants from the Radiological Society of North America Research and Education Foundation and the National Institutes of Health (K01DK099451, R01CA183071, and P41EB013598).

References

1. Kurhanewicz J, Vigneron DB, Brindle K, et al. Analysis of cancer metabolism by imaging hyperpolarized nuclei: prospects for translation to clinical research. Neoplasia. 2011; 13:81–97. [PubMed: 21403835]
2. Schroeder MA, Clarke K, Neubauer S, Tyler DJ. Hyperpolarized magnetic resonance: a Novel technique for the in vivo assessment of cardiovascular disease. Circulation. 2011; 124:1580–1594. [PubMed: 21969318]

3. Chen AP, Lau JYC, Alvares RDA, Cunningham CH. Using [1-(13) C]lactic acid for hyperpolarized (13) C MR cardiac studies. Magn Reson Med. 2015; 73:2087–2093. [PubMed: 25046652]
4. MacKenzie JD, Yen YF, Mayer D, Tropp JS, Hurd RE, Spielman DM. Detection of inflammatory arthritis by using hyperpolarized 13C-pyruvate with MR imaging and spectroscopy. Radiology. 2011; 259:414–420. [PubMed: 21406626]
5. Lee P, Leong W, Tan T, Lim M, Han W, Radda GK. In vivo hyperpolarized carbon-13 magnetic resonance spectroscopy reveals increased pyruvate carboxylase flux in an insulin-resistant mouse model. Hepatology. 2013; 57:515–524. [PubMed: 22911492]
6. Josan S, Billingsley K, Orduna J, Park JM, Luong R, Yu L, Hurd R, Pfefferbaum A, Spielman D, Mayer D. Assessing inflammatory liver injury in an acute CCl4 model using dynamic 3D metabolic imaging of hyperpolarized [1-(13) C]pyruvate. NMR Biomed. 2015; 28(12):1671–1677. [PubMed: 26474216]
7. Tsuda N, Matsui O. Cirrhotic rat liver: reference to transporter activity and morphologic changes in bile canaliculi—gadoxetic acid-enhanced MR imaging. Radiology. 2010; 256:767–773. [PubMed: 20663976]
8. Leonhardt M, Keiser M, Oswald S, Kuhn J, Jia J, Grube M, Kroemer HK, Siegmund W, Weitschies W. Hepatic uptake of the magnetic resonance imaging contrast agent Gd-EOB-DTPA: role of human organic anion transporters. Drug Metab Dispos. 2010; 38:1024–1028. [PubMed: 20406852]
9. van Montfoort JE, Stieger B, Meijer DK, Weinmann HJ, Meier PJ, Fattinger KE. Hepatic uptake of the magnetic resonance imaging contrast agent gadoxetate by the organic anion transporting polypeptide Oatp1. J Pharmacol Exp Ther. 1999; 290:153–157. [PubMed: 10381771]
10. Cruite I, Schroeder M, Merkle EM, Sirlin CB. Gadoxetate disodium-enhanced MRI of the liver: part 2, protocol optimization and lesion appearance in the cirrhotic liver. Am J Roentgenol. 2010; 195:29–41. [PubMed: 20566795]
11. Endrikat JS, Dohanish S, Balzer T, Breuer JAM. Safety of gadoxetate disodium: results from the clinical phase II-III development program and postmarketing surveillance. J Magn Reson Imaging. 2015; 42:634–643. [PubMed: 25643844]
12. Ringe KI, Husarik DB, Sirlin CB, Merkle EM. Gadoxetate disodium-enhanced MRI of the liver. Part 1: protocol optimization and lesion appearance in the noncirrhotic liver. Am J Roentgenol. 2010; 195:13–28. [PubMed: 20566794]
13. Hu S, Zhu M, Yoshihara HAI, et al. In vivo measurement of normal rat intracellular pyruvate and lactate levels after injection of hyperpolarized [1-(13)C]alanine. Magn Reson Imaging. 2011; 29:1035–1040. [PubMed: 21855243]
14. Bashir MR, Breault SR, Braun R, Do RK, Nelson RC, Reeder SB. Optimal timing and diagnostic adequacy of hepatocyte phase imaging with gadoxetate-enhanced liver MRI. Acad Radiol. 2014; 21:726–732. [PubMed: 24717550]
15. Kiryu S, Inoue Y, Watanabe M, Izawa K, Shimada M, Tojo A, Yoshikawa K, Ohtomo K. Evaluation of gadoxetate disodium as a contrast agent for mouse liver imaging: comparison with gadobenate dimeglumine. Magn Reson Imaging. 2009; 27:101–107. [PubMed: 18599243]
16. Rosset A, Spadola L, Ratib O. OsiriX: an open-source software for navigating in multidimensional DICOM images. J Digit Imaging. 2004; 17:205–216. [PubMed: 15534753]
17. Hao D, Ai T, Goerner F, Hu X, Runge VM, Tweedle M. MRI contrast agents: basic chemistry and safety. J Magn Reson Imaging. 2012; 36:1060–1071. [PubMed: 23090917]
18. Cunningham CH, Chen AP, Albers MJ, Kurhanewicz J, Hurd RE, Yen Y-F, Pauly JM, Nelson SJ, Vigneron DB. Double spin-echo sequence for rapid spectroscopic imaging of hyperpolarized 13C. J Magn Reson. 2007; 187:357–362. [PubMed: 17562376]
19. Zhao L, Mulkern R, Tseng C, Williamson D, Patz S, Kraft R, Walsworth R, Jolesz F, Albert M. Gradient-echo imaging considerations for hyperpolarized 129Xe MR. J Magn Reson B. 1996; 113:179–183.
20. Crane JC, Olson MP, Nelson SJ. SIVIC: open-source, standards-based software for DICOM MR spectroscopy workflows. Int J Biomed Imaging. 2013:1–12.
21. van Heeswijk RB, Laus S, Morgenthaler FD, Gruetter R. Relaxivity of Gd-based contrast agents on X nuclei with long intrinsic relaxation times in aqueous solutions. Magn Reson Imaging. 2007; 25:821–825. [PubMed: 17448617]

22. Rodríguez H, Soto A, Arce A. Apparent molar volume, isentropic compressibility, refractive index, and viscosity of DL-alanine in aqueous NaCl solutions. J Solution Chem. 2003; 32(1):53–63.

23. Frankel TL, Gian RK, Jarnagin WR. Preoperative imaging for hepatic resection of colorectal cancer metastasis. J Gastrointest Oncol. 2012; 3:11–18. [PubMed: 22811865]

24. Bellin M-F. MR contrast agents, the old and the new. Eur J Radiol. 2006; 60:314–323. [PubMed: 17005349]

25. Smith MR, Peterson ET, Gordon JW, Niles DJ, Rowland IJ, Kurpad KN, Fain SB. In vivo imaging and spectroscopy of dynamic metabolism using simultaneous 13C and 1H MRI. IEEE Trans Biomed Eng. 2012; 59:45–49. [PubMed: 21775254]

26. Reed GD, von Morze C, Verkman AS, et al. Imaging renal urea handling in rats at millimeter resolution using hyperpolarized magnetic resonance relaxometry. 2015:1–13. arXiv:1511.00200v2 [physics.med-ph].

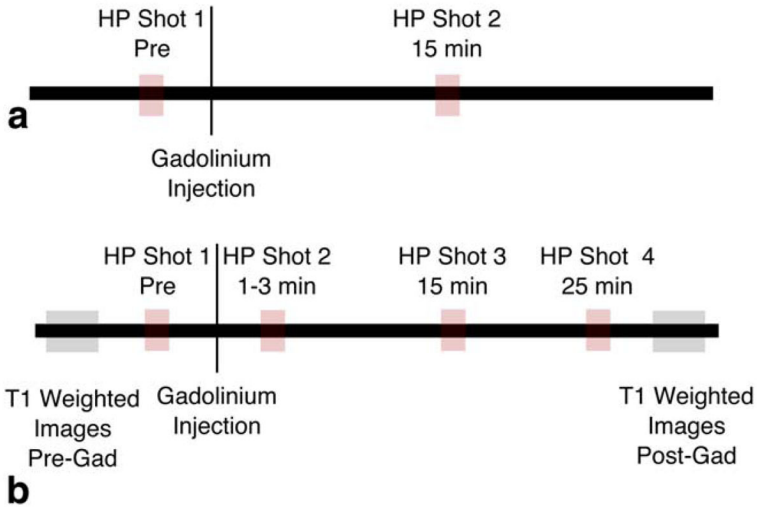

FIG. 1.

Timing of hyperpolarized injections used in this work: (**a**) Timing for slab dynamic imaging; (**b**) timing for 3D echo planar spectroscopic imaging. All times are relative to gadoxetate injection. Each red box represents a separate hyperpolarized ^{13}C-pyruvate injection and acquisition. T_1-weighted images were obtained before and after hyperpolarized ^{13}C imaging to confirm gadoxetate arrival.

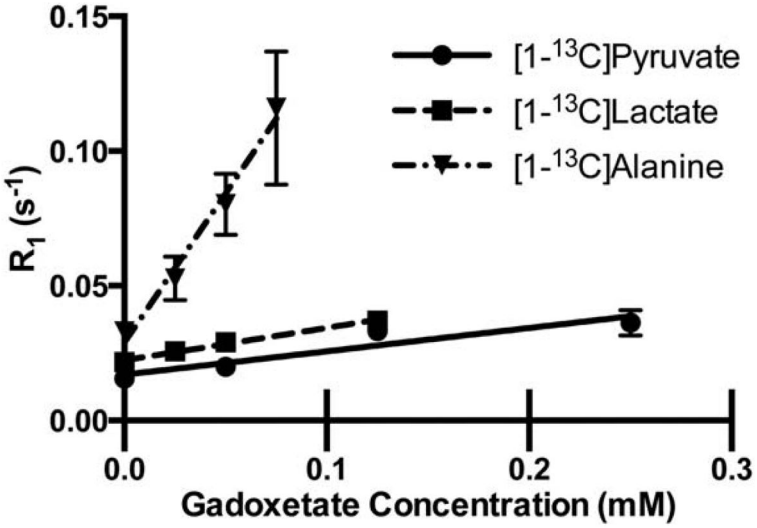

FIG. 2.

Longitudinal relaxation rate, R_1, as a function of gadoxetate concentration for [1-^{13}C]pyruvate and its metabolites. The slope of each plot represents the relaxivity of gadoxetate for that compound. All measurements performed at ~25°C dissolved in phosphate-buffered saline. R_1 of pyruvate and lactate were measured at 24 mM through the signal decay of hyperpolarized sample. R_1 of alanine was measured through saturation recovery of a non-hyperpolarized sample at 1.2 M.

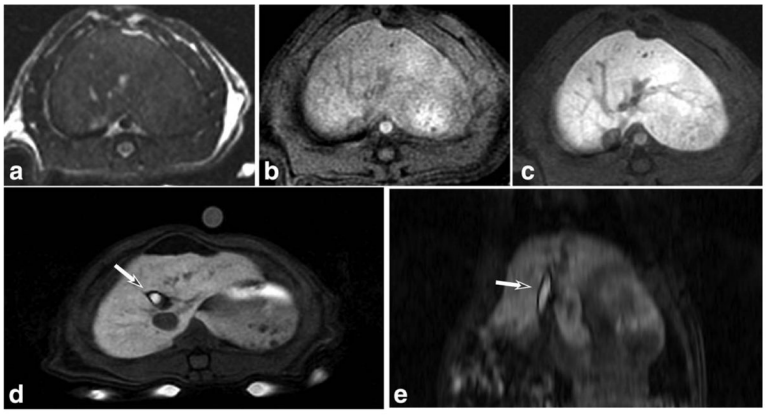

FIG. 3.

Proton imaging used as an anatomic reference and to confirm the arrival of gadoxetate. (**a**) Axial steady-state free precession images through the liver. T_1-weighted spoiled gradient echo images acquired (**b**) before and (**c–e**) approximately 25 min following administration of gadoxetate. (**e**) Coronal reformation of the axial data in (**c–d**). There is expected hyperenhancement of the liver parenchyma relative to the vasculature and muscles. There has been excretion into the common bile duct (arrow), which is characteristic of gadoxetate in the hepatobiliary phase.

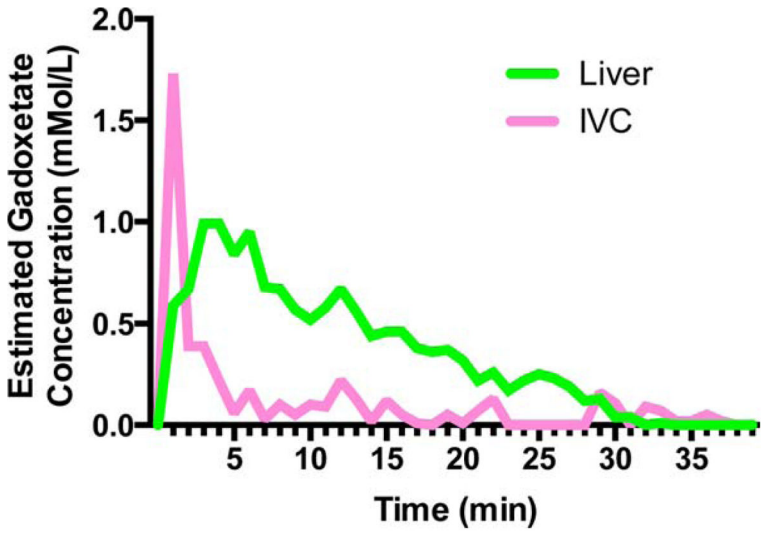

FIG. 4.

Contrast enhancement dynamics following tail vein injection of gadoxetate into a rat at a dose of 0.1 mmol/kg. ROIs were placed over the liver and the IVC.

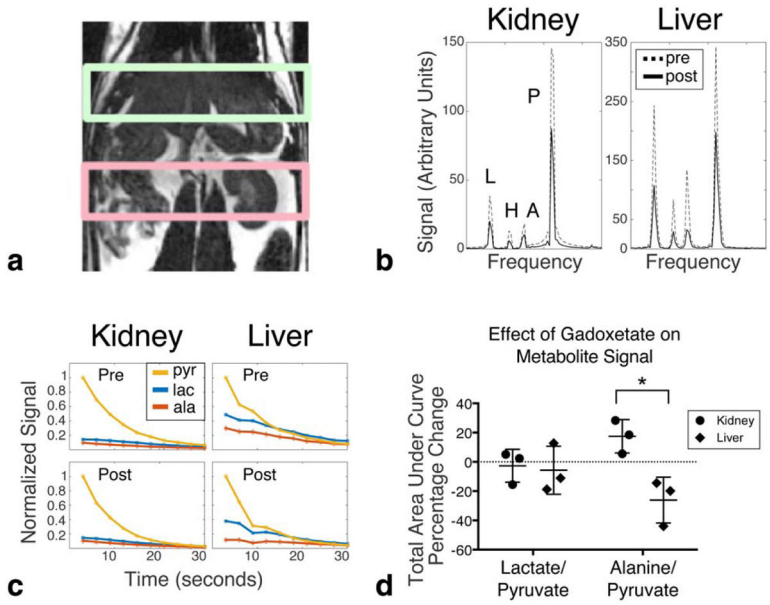

FIG. 5.

Dynamic experiments from 2-cm slabs placed over the liver and kidney. (**a**) Slab locations. (**b**) Summed spectra over all time points for a single animal. Metabolite peaks are labeled as lactate (L), pyruvate hydrate (H), alanine (A), and pyruvate (P). Dotted lines are spectra acquired before gadoxetate administration. Solid lines are spectra acquired 15 min after gadoxetate administration. (**c**) Dynamic time curves for each metabolite beginning 20 s after injection. All curves are normalized so that the initial pyruvate signal is 1. (**d**) Scatter plot comparing the percentage change in total lactate and alanine signal (measured as area under the dynamic curve) in the kidney slab and liver slab before and after gadolinium. Each point on the scatter plot corresponds to a different animal. Error bars are standard deviation. *P <0.05.

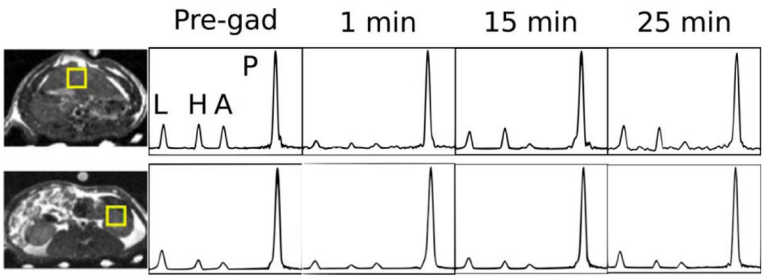

FIG. 6.

Spectra obtained from single voxels placed over the liver (top row) and left kidney (bottom row). The left column shows the location of the voxels overlayed on SSFP anatomic images. Successive columns show spectra obtained before gadoxetate administration and then at various time points after gadoxetate administration. Each spectrum is normalized so that the pyruvate signal is equal to 1. Metabolite peaks are labeled as lactate (L), pyruvate hydrate (H), alanine (A), and pyruvate (P).

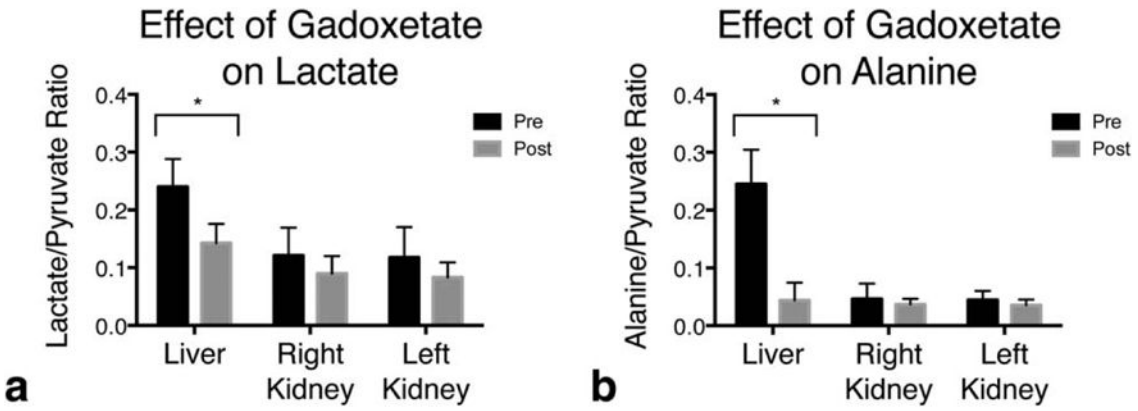

FIG. 7.

Average metabolite levels measured within an ROI placed over the liver or kidneys. “Post” data were acquired 15 min after injection of gadoxetate. *P<0.05. (**a**) Lactate/pyruvate ratio; (**b**) alanine/pyruvate ratio. Error bars are standard deviation (n = 4).

Table 1

Relaxivity of Gadoxetate With Respect to [1-^{13}C]Pyruvate and Its Metabolites Dissolved in Phosphate-Buffered Saline

Agent	Relaxivity (mM^{-1} s^{-1})
[1-^{13}C]pyruvate	0.087 +/−0.023
[1-^{13}C]lactate	0.12 +/−0.008
[1-^{13}C]alanine	1.11 +/− 0.103[a]

Note: Pyruvate and lactate relaxivity were measured at a concentration of 24 mM using a hyperpolarized sample. Alanine relaxivity was measured at a concentration of 1.2 M using a non-hyperpolarized sample and saturation recovery (see text).

[a]The relaxivity of alanine differed significantly (P <0.05) from that of pyruvate and lactate.